Available online at www.sciencedirect.com
SCIENCE DIRECT®
Journal of Magnetic Resonance 163 (2003) 81–91
JMR Journal of Magnetic Resonance
www.elsevier.com/locate/jmr

CPMG relaxation by diffusion with constant magnetic field gradient in a restricted geometry: numerical simulation and application

Gigi Q. Zhang[a,*] and George J. Hirasaki[b]

[a] *Baker Hughes Incorporated, Houston, TX, USA*
[b] *Rice University, Houston, TX, USA*

Received 2 December 2002; revised 21 March 2003

Abstract

Carr–Purcell–Meiboom–Gill (CPMG) measurements are the primary nuclear magnetic resonance (NMR) technique used for evaluating formation properties and reservoir fluid properties in the well logging industry and laboratory sample analysis. The estimation of bulk volume irreducible (BVI), permeability, and fluid type relies on the accurate interpretation of the spin–spin relaxation time (T_2) distribution. The interpretation is complicated when spin's self-diffusion in an inhomogeneous field and restricted geometry becomes dominant. The combined effects of field gradient, diffusion, and a restricted geometry are not easily evaluated analytically. We used a numerical method to evaluate the dependence of the free and restricted diffusion on the system parameters in the absence of surface relaxation, which usually can be neglected for the non-wetting fluids (e.g., oil or gas). The parameter space that defines the relaxation process is reduced to two dimensionless groups: D^* and τ^*. Three relaxation regimes: free diffusion, localization, and motionally averaging regimes are identified in the $(\log_{10} D^*,\ \log_{10} \tau^*)$ domain. The hypothesis that the normalized magnetization, $\hat{M}^*$, relaxes as a single exponential with a constant dimensionless relaxation time T_2^* is justified for most regions of the parameter space. The numerical simulation results are compared with the analytical solutions from the contour plots of T_2^*. The locations of the boundaries between different relaxation regimes, derived from equalizing length scales, are challenged by observed discrepancies between numerical and analytical solutions. After adjustment of boundaries by equalizing T_2^*, numerical simulation result and analytical solution match each other for every relaxation regime. The parameters, fluid diffusivity and pore length, can be estimated from analytical solutions in the free diffusion and motionally averaging regimes, respectively. Estimation of the parameters near the boundaries of the regimes may require numerical simulation.

1. Introduction

Carr–Purcell–Meiboom–Gill (CPMG) pulse sequence, as shown in Fig. 1, is widely used to measure spin–spin relaxation time T_2. After the initial $\pi/2$ (or 90°) pulse, spins at different locations rotate around the z axis (the same axis as the static magnetic field B_0) at differing speeds due to the field inhomogeneity. A π (or 180°) pulse is applied (around the rotating imaginary axis) at time τ to refocus the spins, which leads to the formation of the "Hahn" echo at time 2τ. Then further applications of π pulses at $3\tau, 5\tau, \ldots$, the odd multiples of τ, lead to the formation of the CPMG echoes at $4\tau, 6\tau, \ldots$, the even multiples of τ. Only when spins are not diffusing, can CPMG completely compensate the dephasing of spins due to the local magnetic field inhomogeneity.

Many researchers studied the decay of the CPMG spin echo amplitude resulting from the combined effects of field gradients, diffusion, and restricted geometries [1–5].

Hürlimann [6] showed that the pores can be classified into large or small pores, by comparing the pore size to $\sqrt{D_0/\gamma\Delta\chi B_0}$ (D_0 is the molecular self-diffusion coefficient. γ is the gyromagnetic ratio. $\Delta\chi$ is the magnetic susceptibility difference between pore fluid and rock matrix. B_0 is the static magnetic field). Only the contributions from the large pores show a significant increase of the CPMG decay rate with echo spacing TE.

Sen et al. [7] studied the influence of restricted geometry on CPMG spin echo response of the magnetization of spins diffusing in a constant magnetic field gradient. Depending on three main length scales: L_D

* Corresponding author. Fax: 1-713-625-6795.
E-mail address: gigi.zhang@bakerhughes.com (G.Q. Zhang).

1090-7807/03/$ - see front matter © 2003 Elsevier Science (USA). All rights reserved.
doi:10.1016/S1090-7807(03)00108-3

Nomenclature

a_1	a numerical constant in analytical Eq. (9)
A	$m \times m$ tri-diagonal matrix in numerical simulation
B	$m \times m$ tri-diagonal matrix in numerical simulation
B_0	static magnetic field
B_z	the z component of magnetic field
BVI	bulk volume irreducible
C	a numerical constant in analytical Eq. (8), which depends on the echo number n
C_1	a numerical constant in analytical Eq. (9)
C_2	a numerical constant in analytical Eq. (9)
CPMG	Carr–Purcell–Meiboom–Gill
$\Delta\chi$	magnetic susceptibility difference between pore fluid and rock matrix
D_0	molecular self-diffusion coefficient
D^*	dimensionless group, $D^* = \frac{D_0}{\gamma g L_S^2}$
g	constant magnetic field gradient
G	tool gradient
γ	gyromagnetic ratio
h	same as Δx^*
i	imaginary unit
j	grid point index in numerical simulation
L_D	diffusion length
L_g	dephasing length
L_S	system length
m	the number of grid blocks used in the numerical simulation for the 1-D pore
M	magnetization, expressed as a complex variable, $M = M_x + iM_y$
$\hat{M}$	magnetization with the precession at Larmor frequency and the bulk relaxation factored out
$\hat{M}_0$	$\hat{M}$ at time zero
$\hat{M}^*$	normalized magnetization, $\hat{M}^* = \frac{\hat{M}}{\hat{M}_0}$
n	echo number
N	time step index in numerical simulation
N_τ	the number of micro time steps in each τ^* (or τ) interval
nmr	nuclear magnetic resonance
p	a numerical constant in analytical Eq. (9), which depends on the echo number n
π	a radiofrequency pulse that lasts to tip spins by 180°
π_-	at time immediately before a π pulse
π_+	at time immediately after a π pulse
θ	coefficient in Crank–Nicholson finite difference method
t	time
t_0	characteristic time or dephasing time, $t_0 = \frac{1}{\gamma g L_S}$
t^*	dimensionless time, $t^* = \frac{t}{t_0}$
Δt^*	dimensionless time step, $\Delta t^* = t^*_{N+1} - t^*_N$
T_2	spin–spin relaxation time
T_{2B}	bulk spin–spin relaxation time
T_2^*	dimensionless spin–spin relaxation time, $T_2^* = \frac{T_2}{t_0}$
τ	half echo spacing
τ^*	dimensionless group, $\tau^* = \tau\gamma g L_S$
U	time evolution matrix, $U = A^{-1}B$
V_1	defined as $V_1 = U^{N_\tau}$
V_2	defined as $V_2 = -\overline{(U^{N_\tau})}$
$\bar{\omega}_0$	Larmor frequency
x, y, z	Cartesian coordinates
x^*	dimensionless x, $x^* = \frac{x}{L_S}$
Δx^*	dimensionless space between grid points

(diffusion length), L_g (dephasing length), and L_S (system length), three main regimes of decay have been identified: free diffusion, localization, and motionally averaging regimes. They conducted numerical simulations to investigate how spins pass from one regime of relaxation to another, particularly from the localization regime to the motionally averaging regime. In this transition, they observed large oscillations in the CPMG signal as a function of the echo number for certain specific values of echo spacing and the magnetic field gradient.

In this paper, we will re-interpret the differential equation with two dimensionless groups and conduct numerical simulations to study the combined effects of field gradient, diffusion, and restricted geometry on NMR measurements.

Compared with Sen et al.'s work, instead of characterizing T_2 relaxation process in the domain of three dimensional length scales: L_D, L_g, and L_S we propose to study in the domain of two dimensionless groups: D^* and τ^* in a log–log scale. In addition, instead of studying the relaxation process as a function of time or echo number, we propose to use dimensionless relaxation time, T_2^*. Thus, a single contour plot of T_2^* will suffice to describe the whole relaxation process. All three relaxation regimes can be displayed on the $(\log_{10} D^*, \log_{10} \tau^*)$ domain. Analytical equations allow us to derive the boundaries between adjacent relaxation regimes from equalizing the characteristic length scales. However, numerical simulation results challenge the validity of these boundaries. This discrepancy prompts us to adjust the boundaries by equalizing T_2^* of adjacent regimes. Finally, one contour plot of T_2^* from numerical simulation covers all three relaxation regimes, whereas analytical solution occupies only portion of the $(\log_{10} D^*, \log_{10} \tau^*)$ domain.

2. Numerical method

2.1. System of study

The distribution of the magnetic field gradients for natural rock samples can be very complicated. It is the superposition of a constant gradient applied by the

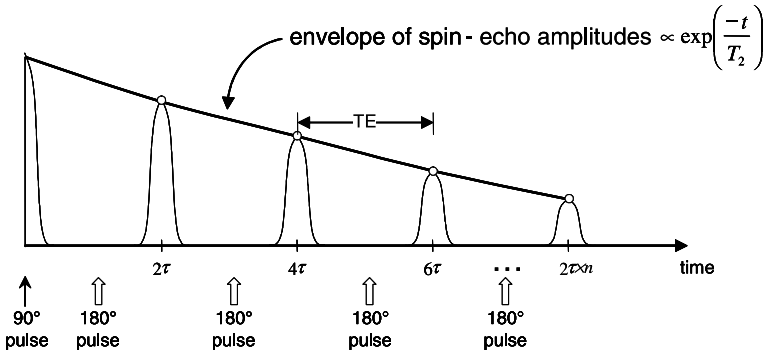

Fig. 1. CPMG pulse sequence. It begins with a 90° pulse followed by a series of 180° pulses. The first two pulses are separated by a time period τ, whereas the remaining pulses are spaced 2τ apart. Echoes occur halfway between 180° pulses at $2\tau, 4\tau, \ldots, 2\tau \times n$, where n is the echo number. TE stands for echo spacing and it equals to 2τ. Spin echo amplitudes decay with the time constant T_2.

logging tool with a distribution of the internal field gradients induced from the magnetic susceptibility difference between pore fluids and solid matrix [8]. Thus, the determination of the NMR response of the magnetization of spins for real systems is a very difficult task. In this paper, we will restrict ourselves to the most fundamental yet important case, i.e., a 1-D system in a magnetic field with constant gradient.

Therefore, as illustrated in Fig. 2, we define our system of study as a 1-D pore (i.e., a slab) along the x (real) axis. The pore is divided into m grid blocks, each represented by a grid point. Also, we only consider a magnetic field with a constant gradient, i.e., $B_z = B_0 + gx$. Spins are free to diffuse through the pore space.

2.2. System of equations

We can get the following equation only after a few mathematical manipulations on the original Torrey's equations [9]:

$$\frac{\partial M}{\partial t} = -\mathrm{i}\gamma B_z M - \frac{M}{T_2} + D_0 \nabla^2 M, \tag{1}$$

where M is magnetization expressed as a complex variable, $M = M_x + \mathrm{i}M_y$. Let $M = \hat{M} \cdot \exp(-\mathrm{i}\omega_0 t + -t/(T_{2B}))$, then $\hat{M}$ represents the magnetization with the precession at Larmor frequency, $\omega_0 = \gamma B_0$, and the bulk relaxation, T_{2B}, factored out.

In addition, introduce normalized magnetization $\hat{M}^* = \hat{M}/\hat{M}_0$, where $\hat{M}_0$ is the magnetization at time zero. Then, at $t = 0$, $\hat{M}^* = 1$. Hence Eq. (1) becomes:

$$\frac{\partial \hat{M}^*}{\partial t} = -\mathrm{i}\gamma(B_z - B_0)\hat{M}^* + D_0 \nabla^2 \hat{M}^*. \tag{2}$$

For our system of study, i.e., a 1-D pore with a constant gradient and self-diffusion, Eq. (2) becomes:

$$\frac{\partial \hat{M}^*}{\partial t} = -\mathrm{i}\gamma g x \hat{M}^* + D_0 \frac{\partial^2 \hat{M}^*}{\partial x^2} \quad \text{for } -\frac{L_S}{2} < x < \frac{L_S}{2} \text{ and } t > 0. \tag{3}$$

Let $x^* = x/L_S$, where L_S is the system length and $t^* = t/t_0$. The characteristic time, t_0, is also called the dephasing time and it is defined as $t_0 \equiv 1/\gamma g L_S$, in unit of time/radian. t_0 represents the time it takes the spins at $x^* = -1/2$ and $x^* = 1/2$ to dephase by 1 rad due to the magnetic field inhomogeneity. A typical value of t_0 is 1.5 ms/radian (with $\gamma = 2.675 \times 10^8\,\mathrm{rad/(T\,s)}$, $g = 25$ G/cm, and $L_S = 10\,\mu\mathrm{m}$). Thus, Eq. (3) becomes:

$$\frac{\partial \hat{M}^*}{\partial t^*} = -\mathrm{i}x^* \hat{M}^* + \frac{D_0}{\gamma g L_S^3} \cdot \frac{\partial^2 \hat{M}^*}{\partial x^{*2}}. \tag{4}$$

We introduce a dimensionless group D^*, defined as:

$$D^* \equiv \frac{D_0}{\gamma g L_S^3} = \frac{\frac{1}{\gamma g L_S}}{\left(\frac{L_S^2}{D_0}\right)} = \frac{\text{“dephasing time”}}{\text{“diffusion time”}}.$$

It is the ratio of the dephasing time in an inhomogeneous field to the diffusion time across a pore of length L_S.

With the definition of D^*, Eq. (4) becomes:

$$\frac{\partial \hat{M}^*}{\partial t^*} = -\mathrm{i}x^* \hat{M}^* + D^* \frac{\partial^2 \hat{M}^*}{\partial x^{*2}}. \tag{5a}$$

The initial condition is:

$$\hat{M}^*(x^*, t^* = 0) = 1. \tag{5b}$$

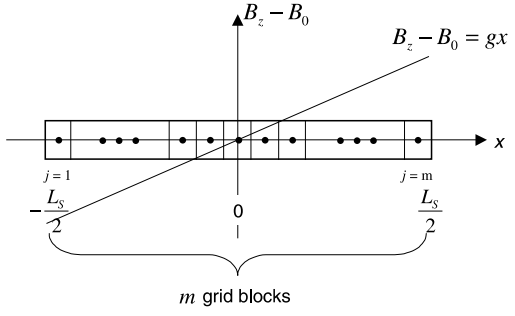

Fig. 2. System of study. A 1-D pore is divided into m grid blocks with total length L_S. It is in the presence of a magnetic field with constant gradient g.

We assume completely reflective pore walls, that is, there is no surface relaxation. This assumption is usually true for non-wetting fluids (e.g., oil or gas). Then, the boundary condition is:

$$\frac{\partial \hat{M}^*}{\partial x^*} = 0 \quad \text{at } x^* = -\frac{1}{2} \text{ and } \frac{1}{2}. \tag{5c}$$

Since CPMG pulse sequence has π pulses at odd numbers of τ: $\tau, 3\tau, \ldots$, we introduce another dimensionless group τ^*, defined as $\tau^* = \frac{\tau}{t_0} = \tau\gamma g L_S$. Then, at $t^* = \tau^*, 3\tau^*, \ldots$, a π pulse is applied.

At each π pulse, the spins are rotated 180° about the y' (rotating imaginary) axis, thus immediately after the π pulse every spin has the same imaginary component, while negative of the real component, as it had immediately before the π pulse. Therefore, the effect of a π pulse can be expressed as the negative of complex conjugate, i.e.:

$$\hat{M}^*_{\pi_+} = -\overline{(\hat{M}^*_{\pi_-})}, \tag{5d}$$

where π_- and π_+ stand for at time immediately before and after a π pulse.

Thus far, the diffusion problem is completely mathematically formulated by the system of Eqs. (5a)–(5d).

By using dimensionless values, we have replaced dimensional variables: $\hat{M}$, t, and x with dimensionless variables: $\hat{M}^*$, t^*, and x^*. More importantly, we reduce the number of dimensional parameters: γ, g, D_0, L_S, $\hat{M}_0$, and τ to only two dimensionless groups: D^* and τ^*.

2.3. Finite difference method

For numerical stability and second order convergence, we use Crank–Nicholson finite difference method to solve the system of Eqs. (5a)–(5d).

In simple matrix form, Eq. (5a) combined with boundary condition (5c) for all the grid blocks can be expressed as:

$$A\hat{M}^{*N+1} = B\hat{M}^{*N}, \tag{6}$$

where A and B are $m \times m$ tri-diagonal matrices and $\hat{M}^{*N+1}$ and $\hat{M}^{*N}$ are $m \times 1$ matrices at time step t^*_{N+1} and t^*_N, respectively. N is the time step index in numerical simulation, $N = 1, 2, \ldots$

Eq. (6) is fully expanded as:

$$\begin{bmatrix} \frac{h^2}{\Delta t^*} + \theta \cdot \mathrm{i}h^2 x_1^* + D^*\theta & -D^*\theta & & & \\ \cdots & \cdots & \cdots & & \\ & -D^*\theta & \frac{h^2}{\Delta t^*} + \theta \cdot \mathrm{i}h^2 x_j^* + 2D^*\theta & -D^*\theta & \\ & & \cdots & \cdots & \cdots \\ & & & -D^*\theta & \frac{h^2}{\Delta t^*} + \theta \cdot \mathrm{i}h^2 x_m^* + D^*\theta \end{bmatrix} \begin{bmatrix} \hat{M}_1^{*N+1} \\ \hat{M}_2^{*N+1} \\ \cdots \\ \hat{M}_{m-1}^{*N+1} \\ \hat{M}_m^{*N+1} \end{bmatrix}$$

$$= \begin{bmatrix} \frac{h^2}{\Delta t^*} - (1-\theta)\mathrm{i}h^2 x_1^* - D^*(1-\theta) & D^*(1-\theta) & & & \\ \cdots & \cdots & \cdots & & \\ & D^*(1-\theta) & \frac{h^2}{\Delta t^*} - (1-\theta)\mathrm{i}h^2 x_j^* - 2D^*(1-\theta) & D^*(1-\theta) & \\ & & \cdots & \cdots & \cdots \\ & & & D^*(1-\theta) & \frac{h^2}{\Delta t^*} - (1-\theta)\mathrm{i}h^2 x_m^* - D^*(1-\theta) \end{bmatrix}$$

$$\begin{bmatrix} \hat{M}_1^{*N} \\ \hat{M}_2^{*N} \\ \cdots \\ \hat{M}_{m-1}^{*N} \\ \hat{M}_m^{*N} \end{bmatrix},$$

where $h = \Delta x^* \equiv x^*_{j+1} - x^*_j = 1/m$, $\Delta t^* = t^*_{N+1} - t^*_N$, and $\theta = 0.5$.

To save computational time, we follow the same procedure as illustrated in Sen's paper [7] to skip calculating $\hat{M}^*$ at the intermediate micro time steps but rather calculate $\hat{M}^*$ at echo time $t^* = 2n\tau^*$, where n is the echo number starting from 1.

Rewrite Eq. (6) as: $\hat{M}^{*N+1} = U\hat{M}^{*N}$, where $U = A^{-1}B$, the time evolution matrix for a single micro time step $\Delta t^* = t^*_{N+1} - t^*_N$. Let the number of micro time steps in each τ^* (or τ) interval be N_τ, i.e., $N_\tau = \tau^*/\Delta t^*$. Now, $N = 1, 2, \ldots, N_\tau$. The dimensionless normalized magnetization immediately before the first π pulse is: $\hat{M}^{*N_\tau} = U^{N_\tau}\hat{M}^{*0}$, where $\hat{M}^{*0} = 1$ is the initial condition. Define $V_1 = U^{N_\tau}$ and $V_2 = -\overline{(U^{N_\tau})}$. As stated in the previous section, the effect of a π pulse is negative conjugate (Eq. (5d)). We further assume that the pulse length is infinitesimally small. Then, at $t^* = 2\tau^*$, when the Hahn echo forms, $\hat{M}^{*2N_\tau} = U^{N_\tau}\lfloor -(\hat{M}^{*N_\tau})\rfloor = V_1V_2(\hat{M}^{*0})$. Similarly, the recursive formula for all the echoes is:

$$\hat{M}^{*n} = V_1V_2\overline{(\hat{M}^{*n-1})},$$

where n is the echo number starting from 1. Therefore, the matrix V_1V_2 only needs to be computed once, thus saving a lot of computational time.

It is obvious from the system of equations that CPMG in a 1-D system with a constant gradient and self-diffusion is solely governed by two dimensionless groups: D^* and τ^*. We choose a domain of D^* (ranging from 10^{-4} to 10^2) and τ^* (ranging from 10^{-1} to $10^{1.5}$), which covers the typical combinations of the dimensional parameters: D_0, g, L_S, and τ that are often encountered in real systems. A mesh grid of 121 by 121 points on the $(\log_{10} D^*, \log_{10} \tau^*)$ domain is chosen in later analysis.

To get accurate numerical simulation results, we need to have large numbers of grid blocks and small time step size in order to reach the acceptable levels of spatial and time truncation errors for the whole $(\log_{10} D^*, \log_{10} \tau^*)$ domain. It is founded that 99 grid blocks and 512 micro time steps in each τ^* interval are sufficient for all regions on the $(\log_{10} D^*, \log_{10} \tau^*)$ domain.

3. Numerical results

People usually study the decay of magnetization along time scale or as a function of echo number [7]. Then contour plots of $\hat{M}^*$ need to be created at a series of time values to understand the whole relaxation process. Alternatively, we express $\hat{M}^*$ as relaxing exponentially with t^*, characterized by a constant relaxation time T_2^*:

$$\hat{M}^*(t^*) = \mathrm{e}^{-\frac{t^*}{T_2^*}} \text{ or } T_2^* = \frac{-t^*}{\ln \hat{M}^*(t^*)}.$$

This dimensionless relaxation time, T_2^*, is defined as the ratio of the dimensional relaxation time to the dephasing time, i.e., $T_2^* = T_2/t_0$. This T_2^* is solely due to the diffusion relaxation mechanism. This is because the bulk relaxation is factored out in the beginning to get $\hat{M}$ from M and in the current study, we assume there is no surface relaxation on the pore wall.

If T_2^* determined from the numerical simulation does not change with time, then the relaxation of magnetization follows the single exponential model. Fig. 3 compares contour lines of T_2^* at two different times. Solid curves are at $t^* = 80$, while dashed curves are at $t^* = 800$. Except for the upper left region (due to the branch point effect of the localization regime which will be discussed later), the contour lines of T_2^* at these two times overlay on each other very well. This means that for most regions in the domain, $\hat{M}^*$ decays single exponentially. The significance of this finding is that now only one single contour plot of T_2^*, no matter at what time, is enough to characterize the whole relaxation process.

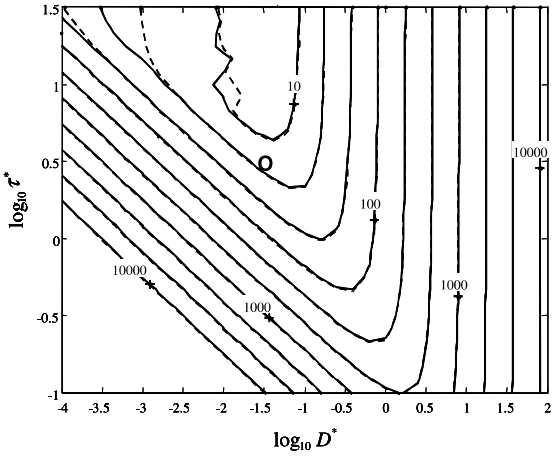

Fig. 3. Comparison of contour lines of T_2^* at $t^* = 80$, solid curves, and at $t^* = 800$, dashed curves.

The contour lines of T_2^* at $t^* = 400 \times (2\tau^*_{\min}) = 80$, the solid curves on Fig. 3, will represent the numerical simulation results referred to in the later discussion. At this time, systems represented by the bottom line of the domain ($\log_{10} \tau^* = -1$) form the 400th echo. Ten contour lines of T_2^* are picked logarithmically from $T_2^* = 10$ (fast relaxation) to $T_2^* = 10,000$ (slow relaxation). They are V-shaped over most of the $(\log_{10} D^*, \log_{10} \tau^*)$ domain.

4. Relaxation regimes of the parameter space

By the way we define the system of equations, there are only two dimensionless groups: D^* and τ^* in the parameter space. Whereas, in the literature [10–12], NMR signal of nuclear magnetization due to restricted diffusion in an inhomogeneous magnetic field is often characterized by three length scales. They are: the system length, L_S, the diffusion length, $L_D \equiv \sqrt{D_0 \tau}$, and the dephasing length, $L_g \equiv (D_0/\gamma g)^{(1/3)}$. The diffusion length is a measure of the distance traveled by a spin in the half echo time τ. The dephasing length is the length over which a spin has to diffuse to dephase by 1 rad. In this way, these three length scales will be needed to completely describe the diffusion problem. Therefore, we reduce the number of parameters from three to two, which is an important improvement that makes the problem much more straightforward.

Three relaxation regimes based on the smallest length scales are identified and their governing analytical equations are given in the literature. A brief summary of these analytical results is given below, where the original analytical equations are expressed in our newly defined parameters: D^* and τ^*.

4.1. Free diffusion regime

L_D is the smallest of the three length scales. Spins are undergoing unrestricted, free diffusion (applies only to the shortest times), as described by Hahn's formula [13]:

$$\hat{M}^*(t^*) = \mathrm{e}^{-(2/3)nD^*\tau^{*3}}. \quad (7)$$

When considering short times after a few spins make contact with the pore walls, Hahn's formula needs to be corrected to the first order due to the wall effect [7,10]:

$$\hat{M}^*(t^*) = \mathrm{e}^{-(2/3)D^*\tau^{*3}\left[n+C(n)\sqrt{D^*\tau^*}\right]}, \tag{8}$$

where $C(n)$ is a numerical constant depending on the echo number n.

4.2. Localization regime

L_g is the smallest of the three length scales. The main characteristic of this regime is that the net signal comes principally from the spins which are within one dephasing length of the boundaries. The attenuation of nuclear magnetization in this regime is given by [7,10,12]:

$$\hat{M}^*(t^*) = p(n)D^{*3}\mathrm{e}^{-a_1 nD^{*\frac{1}{3}}\tau^*}, \tag{9}$$

where $a_1 = 1.0188$. The numerical constants $p(n)$ are:

$$p(n) = 2C_1^n \mathrm{Real}\left[C_2^2\left(\frac{\overline{C_2}}{C_2}\right)^{\mathrm{mod}(n,2)}\right],$$

where $C_1 = 1.31477$ and $C_2 = 1.44545 - 0.387306 * \mathrm{i}$. These $p(n)$ values are for the values of the gradient away from the branch points [14].

4.3. Motionally averaging regime

L_S is the smallest of the three length scales. The spins typically diffuse several times the pore size, and any magnetic field inhomogeneities are averaged out by their motion. The signal decays according to [7]:

$$\hat{M}^*(t^*) = \exp\left\{-\frac{n}{60}\frac{\tau^*}{D^*}\times\left[1-\frac{17}{112}\frac{2n+1}{3n}\frac{1}{D^*\tau^*}\right]\right\}. \tag{10}$$

5. Boundaries from equalizing length scales

Since the most distinct attribute of each relaxation regime is which length scale is the smallest, we derive the boundaries between different relaxation regimes based on this criteria. As illustrated in Fig. 4, three lines, that correspond to the equality between any two length scales (Table 1), divide the $(\log_{10} D^*, \log_{10}\tau^*)$ domain into six regions and they intersect at point $\mathrm{O}(0,0)$ (in log–log scale). The inequality of the three length scales for each region is shown on the figure. Region BCDO has L_D as the smallest length scale, so it is the free diffusion regime. Region ABOG has L_g as the smallest, so it is the localization regime. Region GODEF has L_S as the smallest, so it is the motionally averaging regime. The boundaries between different regimes are marked as solid lines, while dashed lines are extension of these boundaries.

6. Numerical vs. analytical with boundaries from equalizing length scales

In Section 4, we listed the analytical equations (Eqs. (7)–(10)) that describe the three asymptotic regimes of relaxation. In this section we will compare our numerical simulation results with each of them. Contour lines of T_2^* from analytical equation will be shown only for the region where it applies and in the central main plot, while the numerical simulation results will be shown for comparison at the corner.

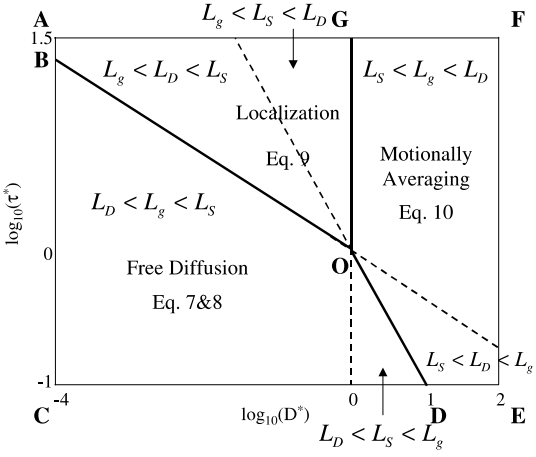

Fig. 4. Boundaries between different relaxation regimes by equalizing length scales. The free diffusion regime, region BCDO, has the smallest L_D; the localization regime, region ABOG, has the smallest L_g; the motionally averaging regime, region GODEF, has the smallest L_S.

Table 1
Boundaries from equalizing length scales

Boundary between	Criteria	Boundary
Free diffusion and motionally averaging	$L_D = L_S$	$\log_{10}\tau^* = -\log_{10} D^*$
Free diffusion and localization	$L_D = L_g$	$\log_{10}\tau^* = -\frac{1}{3}\log_{10} D^*$
Localization and motionally averaging	$L_g = L_S$	$0 = \log_{10} D^*$

For the free diffusion regime, in Fig. 5, numerical simulation shows that contour lines of T_2^* curve up at larger D^*, while analytical equation predicts straight lines throughout the whole region. In Fig. 6, numerical result and analytical solution do not match near the boundary OD. Close observation reveals that numerical simulation predicts curving-up points at smaller D^* values.

For the localization regime, there is an apparent discrepancy between the numerical result and analytical solution, as shown in Fig. 7.

For the motionally averaging regime, numerical result and analytical solution match with each other very well, as shown in Fig. 8.

7. Adjustment of boundaries between relaxation regimes

The discrepancies between numerical result and analytical solution observed for the free diffusion and localization regimes prompt us to examine the validity of

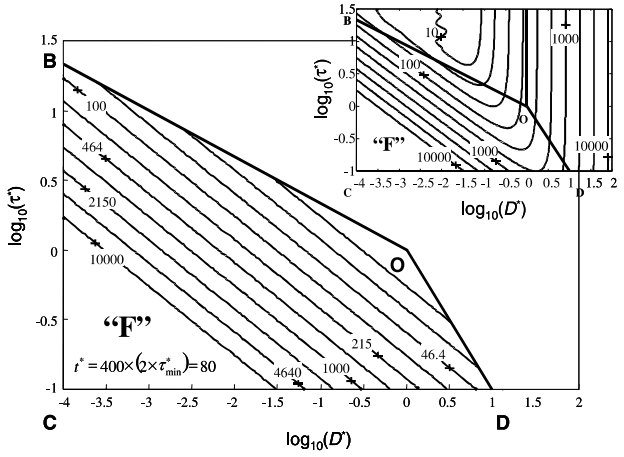

Fig. 5. Contour lines of T_2^* from Eq. (7) plotted for region BCDO vs. numerical results shown at the upper right-hand corner.

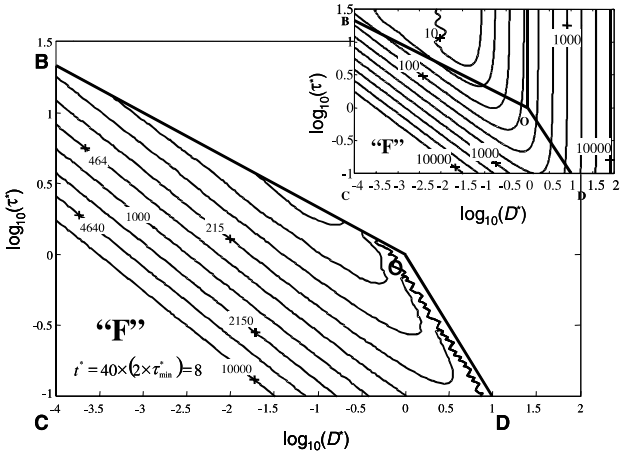

Fig. 6. Contour lines of T_2^* from Eq. (8) plotted for region BCDO vs. numerical results shown at the upper right-hand corner.

the boundaries between different relaxation regimes. Furthermore, it appears that the large D^* portion of the localization regime of the numerical result is an extension of the motionally averaging region.

Let us express the analytical equations in the same form as the numerical simulation:

$$\hat{M}^*(t^*) = e^{-\frac{t^*}{T_2^*}},$$

where $t^* = 2n\tau^*$ and T_2^* is the dimensionless relaxation time.

Then, for the free diffusion regime, we have:

$$\frac{1}{T_2^*} = \frac{1}{3}D^*\tau^{*2}. \tag{11}$$

For the localization regime, rearrange Eq. (9) to have:

$$\hat{M}^*(t^*) = 2\mathrm{Real}\left[C_2^2\left(\frac{\overline{C_2}}{C_2}\right)^{\mathrm{mod}(n,2)}\right]D^{*3}e^{\left(\frac{\ln C_1}{2\tau^*}-\frac{1}{2}a_1D^{*\frac{1}{3}}\right)t^*}. \tag{12}$$

When the L_g is the smallest length scale, the term $(\ln C_1)/2\tau^*$ is usually small compared with $\frac{1}{2}a_1D^{*1/3}$ (see Appendix A for details). Therefore, $1/T_2^*$ can be approximated as:

$$\frac{1}{T_2^*} = \frac{1}{2}a_1D^{*\frac{1}{3}}. \tag{13}$$

For the motionally averaging regime, by ignoring the second term of the exponent in Eq. (10) (justifiable by Fig. 8 where it can be observed that the dimensionless relaxation rate is independent of τ^* for most of the region), the dimensionless relaxation rate can be expressed as:

$$\frac{1}{T_2^*} = \frac{1}{120D^*}. \tag{14}$$

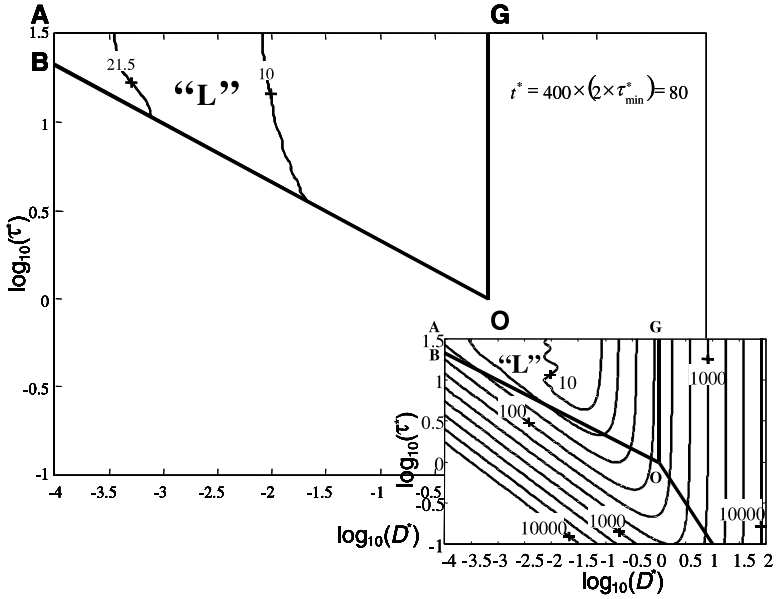

Fig. 7. Contour lines of T_2^* from Eq. (9) plotted for region ABOG vs. numerical results shown at the lower right-hand corner.

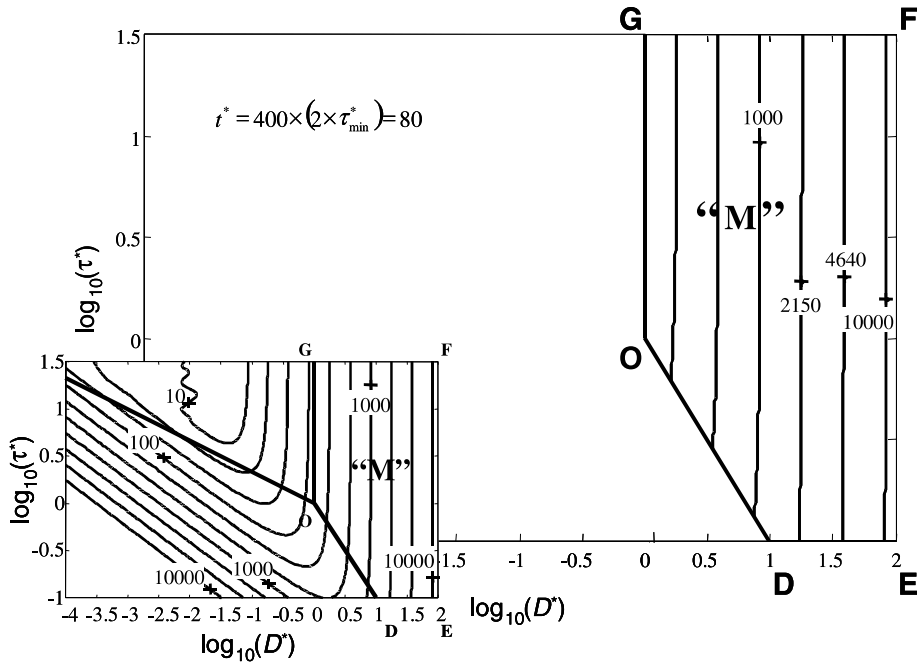

Fig. 8. Contour lines of T_2^* from Eq. (10) plotted for region GODEF vs. numerical results shown at the lower left-hand corner.

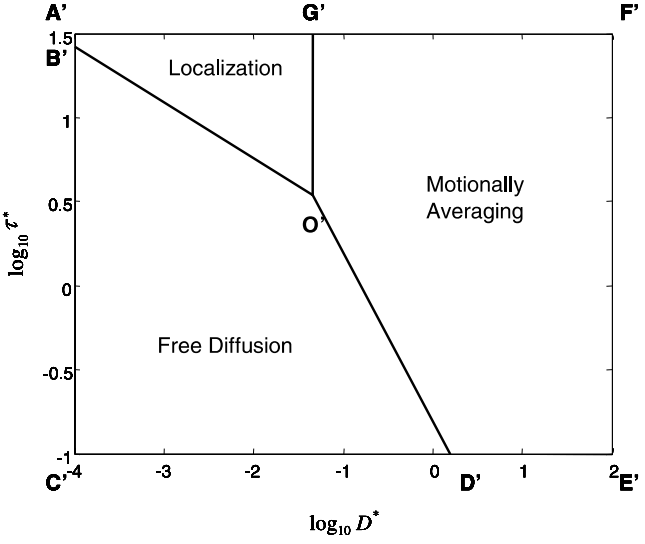

Fig. 9. Adjusted boundaries between different relaxation regimes. They are derived by equalizing T_2^*.

Thus, the boundary between the free diffusion regime and the localization regime can be solved by equalizing Eqs. (11)–(13) as:

$$\log_{10}\tau^* = -\frac{1}{3}\log_{10} D^* + 0.0921. \tag{15}$$

Similarly, the boundary between the localization regime and the motionally averaging regime, derived from equalizing Eq. (13) to Eq. (14), is:

$$\log_{10} D^* = -1.3397 \tag{16}$$

and that between the free diffusion regime (Eq. (11)) and the motionally averaging regime (Eq. (14)) is:

$$\log_{10}\tau^* = -\log_{10} D^* - 0.801. \tag{17}$$

Fig. 9 illustrates the adjusted boundaries derived from equalizing T_2^*. Boundary O′B′ has a slope of −1/3, O′D′ a slope of −1, and O′G′ a vertical line. They intersect at point O′ (−1.3397, 0.5387). Table 2 summarizes the results.

8. Numerical vs. analytical with boundaries from equalizing T_2^*

With new boundaries derived from equalizing T_2^*, numerical simulation is compared with analytical solution in Fig. 10. The upper plot is the contour lines of T_2^* determined from the numerical simulation, while the four lower plots are those calculated from each analytical equation shown only within the newly derived boundaries of each relaxation regime.

Eq. (7) is for the free diffusion regime where contour lines of T_2^* are straight lines with slope $-1/2$. By comparing with the numerical simulation results, it can be concluded that the straight line portion of the numerical results matches very well with the analytical solution.

Eq. (8) of the free diffusion regime is the first order correction to Eq. (7) to account for the partial wall effect. At smaller D^*, the straight line part of Eq. (8) is similar to that of Eq. (7) but with a slope not exactly equal to $-1/2$. Then at larger D^*, the contour lines begin to curve up. Numerical results match the analytical solutions.

For the localization regime, sparsely spaced and wiggling contour lines are both observed on the numerical simulation results and the analytical solutions.

Table 2
Boundaries from equalizing T_2^*

Boundary between	Criteria	Boundary
Free diffusion and motionally averaging	Eq. (11) = Eq. (14)	$\log_{10}\tau^* = -\log_{10} D^* - 0.801$
Free diffusion and localization	Eq. (11) = Eq. (13)	$\log_{10}\tau^* = -\frac{1}{3}\log_{10} D^* + 0.0921$
Localization and motionally averaging	Eq. (13) = Eq. (14)	$\log_{10} D^* = -1.3397$

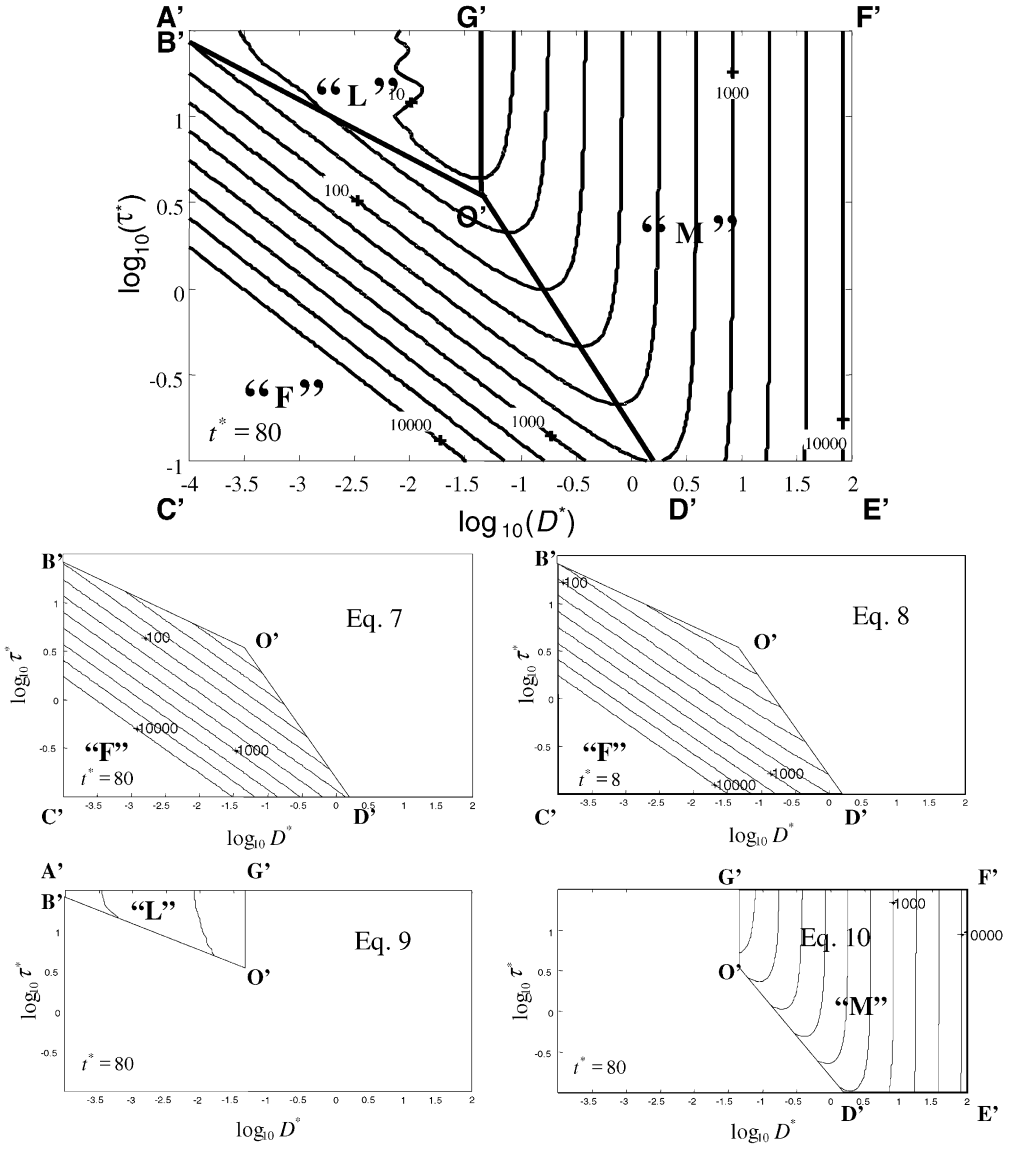

Fig. 10. Comparison of numerical simulation results with analytical solutions with new boundaries derived from equalizing T_2^*.

Numerical results and analytical solutions also match very well for the motionally averaging regime by exhibiting nearly vertical contour lines of T_2^*.

In a word, numerical simulation results match well with the analytical solutions with the adjusted boundaries. Although each analytical solution is valid only in a limited region, the numerical simulation predicts relaxation time for every region in the $(\log_{10} D^*, \log_{10}\tau^*)$ domain. Therefore, one figure from numerical simulation suffices four figures from analytical analysis.

9. Branch point effect in the localization regime

From Fig. 3, it can be observed that the contour lines of T_2^* have a wiggling form and changes with echo number for the localization regime. Similar behavior was observed by other researchers [10,14] who have found that oscillations in the echo signal become large near branch points.

Briefly speaking, with magnetic field gradient $g = 0$, the eigenvalues of the diffusion problem, Eq. (5a), are

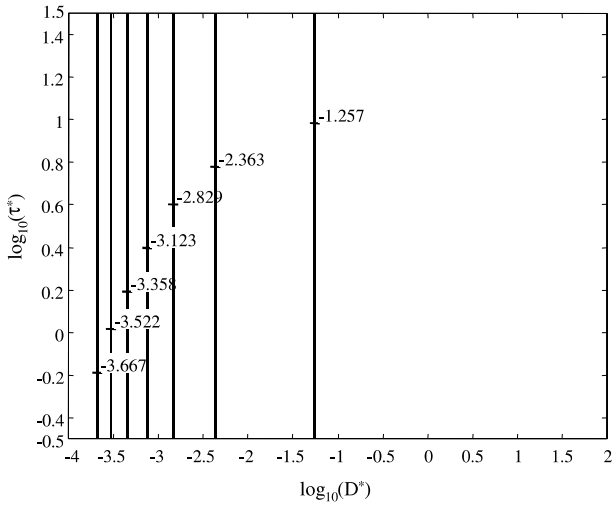

Fig. 11. Vertical branch point lines on the $(\log_{10} D^*, \log_{10} \tau^*)$ domain.

real. As g increases along the positive real axis, eigenvalues shift, and successive pairs of the real-valued eigenvalues coalesce at branch points to form complex conjugate pairs. The branch points occur at special values of the gradient, which in our notation, correspond to certain values of D^*, i.e., $\log_{10} D^* = [-1.257\ -2.363\ -2.829\ -3.123\ -3.358\ -3.522\ -3.667]$.

Fig. 11 plots these vertical branch point lines on the $(\log_{10} D^*, \log_{10} \tau^*)$ domain. Note that the localization regime is densely distributed with branch point lines.

10. Application: determination of D_0 and L_S

The numerical simulator, together with the analytical equations, can be used to determine fluid diffusivity and pore length for systems relaxing at different relaxation regimes.

Fig. 12 plots $1/T_2^*$ over a range of τ^* on a log–log scale at fixed D^*. Six solid lines are for smaller $\log_{10} D^*$ values of [−4 −3.5 −3 −2.5 −2 −1.5]. As τ^* increases (at fixed D^*), nuclear magnetization first relaxes in the free diffusion regime then in the localization regime. So at smaller τ^*, straight lines with slope 2 are observed, then at larger τ^* wiggling curves are seen. Three dashed lines are for intermediate $\log_{10} D^*$ values of [−1 −0.5 0]. They are in the transitional region between the free diffusion regime and the motionally averaging regime. So, they are first straight (slope 2) and then gradually level off. Four dotted lines are for larger $\log_{10} D^*$ values of [0.5 1 1.5 2]. Magnetization relaxes in the motionally averaging regime and the relaxation rate is independent of τ^*. Therefore, horizontal lines are observed.

In practical applications, T_2 measurements at different echo spacings with an applied constant gradient are often performed. So alternatively, $1/T_2$ (note: only consider the relaxation rate due to diffusion mechanism) can be plotted over a range of τ on a log–log scale. The only difference of such plot from Fig. 12 will be a translational shift (by the amount of $\log_{10} t_0$) of the curves while keeping the same shape. Depending on the shape of the curves, fluid diffusivity, D_0, and system length, L_S, can be determined as follows:

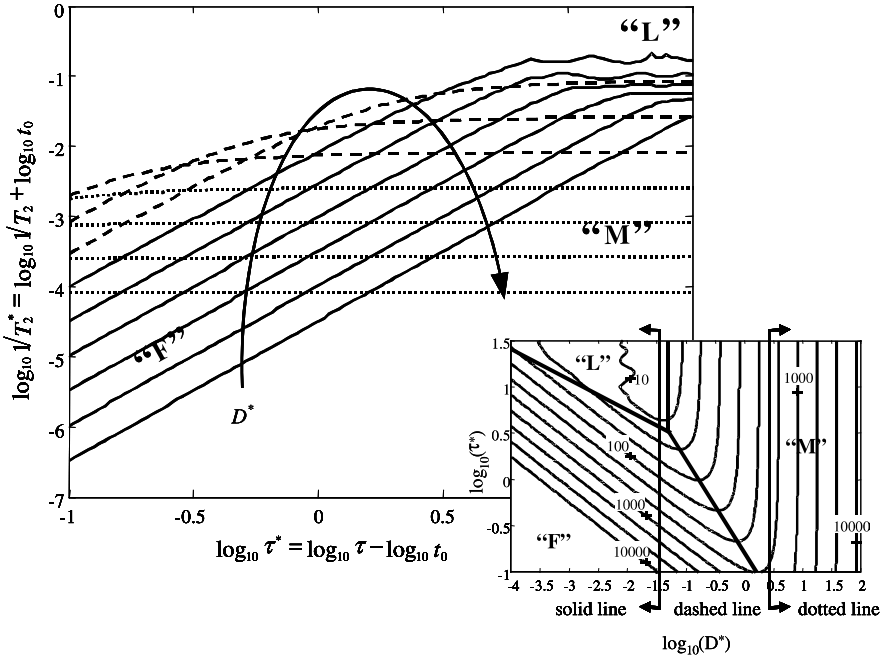

Fig. 12. Relaxation rate vs. half echo spacing on a log–log plot. Straight lines with slope 2 are observed for free diffusion regime and horizontal lines for motionally averaging regime.

1. If a straight line with slope 2 is observed, magnetization decays in the free diffusion regime. From the analytical Eq. (11), the dimensionless relaxation rate is:

$$\frac{1}{T_2^*} = \frac{1}{3} D^* \tau^{*2}.$$

Thus, fluid diffusivity can be determined from T_2, half echo spacing τ, and tool gradient G as :

$$D_0 = \frac{3}{T_2(\gamma \tau G)^2}. \tag{18}$$

2. If a horizontal line is observed, then magnetization decays in the motionally averaging regime as described by Eq. (14):

$$\frac{1}{T_2^*} = \frac{1}{120 D^*}.$$

Therefore, the system length can be determined from D, tool gradient G, and T_2 as:

$$L_S = \left(\frac{120 D_0}{\gamma^2 G^2 T_2} \right)^{\frac{1}{4}}. \tag{19}$$

3. If magnetization decays in the transitional region, then numerical simulator is needed. Just as the analytical Eqs. (11) and (14) where T_2^* is explicitly expressed as a function of D^* and τ^*, numerical simulator implicitly expresses T_2^* as a function of the same two parameters. Thus in principle, both D_0 and L_S can be determined in the transition region.

11. Conclusions

A numerical method for simulating CPMG with self-diffusion was systematically developed. The parameter space that defines the relaxation process can be reduced to two dimensionless groups: D^* and τ^*, instead of three characteristic length scales. Three relaxation regimes: free diffusion, localization, and motionally averaging regimes are identified in the $(\log_{10} D^*, \log_{10} \tau^*)$ domain. Numerical simulation shows that the dimensionless normalized magnetization $\hat{M}^*$ relaxes single exponentially with a constant dimensionless relaxation time T_2^* for most regions of the parameter space except for the localization regime. This result is consistent with the analytical solution.

The analytical and numerical solutions are compared from the contour plots of T_2^*. With boundaries derived from equalizing length scales, discrepancies are observed for free diffusion and localization regimes. However, with adjusted boundaries derived from equalizing T_2^*, analytical and numerical solutions match each other very well for every relaxation regime. Each analytical equation only describes relaxation process in a certain regime, while one numerical simulation covers all three relaxation regimes.

The parameters, fluid diffusivity and pore length, can be estimated from analytical solutions in the free diffusion regime and in the motionally averaging regime, respectively. Estimation of these parameters in the transitional regions will require the numerical simulator.

Acknowledgments

The authors wish to thank for the financial support from the US Department of Energy, Energy, and Environmental Systems Institute of Rice University, and an industrial consortium of Arco, Baker Atlas, ChevronTexaco, ConocoPhillips, Core Labs, ExxonMobil, GRI, Halliburton, Kerr McGee, Marathon, Mobil, Norsk Hydro, Saga, Schlumberger, and Shell.

Appendix A

In order to ignore the first term of the exponent in Eq. (12), $(\ln C_1)/2\tau^*$, it is required that

$$\frac{\ln C_1}{2\tau^*} \ll \frac{1}{2} a_1 D^{*1/3},$$

where $C_1 = 1.31477$ and $a_1 = 1.0188$.

This gives

$$\tau^* D^{*1/3} \gg \frac{\ln C_1}{a_1} = 0.2686.$$

It is equivalent to

$$\log_{10} \tau^* \gg -\frac{1}{3} \log_{10} D^* - 0.57. \tag{A.1}$$

Because the localization regime is above the free diffusion–localization boundary (Eq. (15)) at

$$\log_{10} \tau^* = -\frac{1}{3} \log_{10} D^* + 0.0921,$$

it automatically satisfies the requirement as stated in Eq. (A.1) Therefore, the term, $(\ln C_1)/2\tau^*$, can be ignored from the exponent in Eq. (12).

References

[1] R.L. Kleinberg, M.A. Horsfield, J. Magn. Reson. 88 (1) (1990) 9–19.
[2] P. Le Doussal, P.N. Sen, Phys. Rev. B 46 (1992) 3465.
[3] R.J.S. Brown, P. Fantazzini, Phys. Rev. B 47 (22) (1993) 14823–14834.
[4] D.J. Bergman, K.J. Dunn, Phys. Rev. E 51 (1995) 3401.
[5] D.J. Bergman, K.J. Dunn, G.A. LaTorraca, Bull. Am. Phys. Soc. 40 (1) (1995) 695.
[6] M.D. Hürlimann, J. Magn. Reson. 131 (1998) 232.
[7] P.N. Sen, A. André, S. Axelrod, J. Chem. Phys. 11 (14) (1999) 6548–6555.
[8] G.Q. Zhang, G.J. Hirasaki, W.V. House, paper AA, Society of Professional Well Log Analysts 41st Annual Logging Symposium, Dallas, TX, June 4–7, 2000.
[9] H.C. Torrey, Phys. Rev. 104 (1956) 563.
[10] T.M. deSwiet, P.N. Sen, J. Chem. Phys. 100 (1994) 5597.
[11] K.G. Helmer, M.D. Hürlimann, T.M. de Swiet, P.N. Sen, C.H. Sotak, J. Magn. Reson. A 115 (1995) 257.
[12] M.D. Hürlimann, K.G. Helmer, T.M. de Swiet, P.N. Sen, C.H. Sotak, J. Magn. Reson. A 113 (1995) 260.
[13] E.L. Hahn, Phys. Rev. 80 (1950) 580.
[14] S.D. Stoller, W. Happer, F.J. Dyson, Phys. Rev. A 44 (1991) 7459.